Electronic structure and hyperfine parameters of substitutional Al and P impurities in silica

Lægsgaard, Jesper; Stokbro, Kurt

Published in:
Physical Review B (Condensed Matter and Materials Physics)

Link to article, DOI:
10.1103/PhysRevB.65.075208

Publication date:
2002

Document Version
Publisher's PDF, also known as Version of record

Electronic structure and hyperfine parameters of substitutional Al and P impurities in silica

J. Lægsgaard[1] and K. Stokbro[2]
[1]*Research Center for Communication, Optics, and Materials (COM), Technical University of Denmark, Building 349, DK-2800 Lyngby, Denmark*
[2]*Mikroelektronik Centret, Technical University of Denmark, Building 345 East, DK-2800 Lyngby, Denmark*
(Received 11 December 2000; revised manuscript received 14 March 2001; published 31 January 2002)

The electronic structure of substitutional Al and P impurities in silica is investigated using supercell calculations within the framework of density functional theory (DFT). Evaluation of hyperfine matrices for the magnetic nuclei facilitates comparison to experimental data. It is found that the unpaired spin state of substitutional P is well described by the theory, while the unpaired spin state found for substitutional Al is severely at variance with the experimental data. Cluster calculations using both the DFT and the Hartree-Fock approximation indicate that the problem is not caused by the supercell approach but rather by the residual self-interactions present in the DFT energy functionals. A simple model discussion serves to illustrate why DFT succeeds for P but fails for Al: First, it is argued that DFT self-interactions are larger for holes than for electrons. Second, there is an ''asymmetry'' between electrons and holes in the electronic states of the silica network: The hole present at the Al impurity goes into a nonbonding O orbital while the extra electron present at the P impurity goes into a P-O antibonding state.

DOI: 10.1103/PhysRevB.65.075208 PACS number(s): 61.72.Hh, 71.20.Ps, 76.30.Lh

I. INTRODUCTION

Doped silica glass is a key material for optical communication technology, and there is currently great interest in improving the fundamental understanding of impurity chemistry in silica. Two of the technologically most important dopants are the horizontal neighbors of Si in the periodic table, Al and P. P doping has been used extensively to modify the elastic properties and refractive index of silica glasses, and it has been shown that implantation of P ions can significantly enhance the nonlinear parts of the optical susceptibility.[1] Both Al and P doping have been found to enhance the solubility of rare-earth-metal ions in silica (which is essentially zero in the absence of such codoping), and this effect is of great practical importance in the fabrication of, e.g., light-amplifying optical devices.

A number of experimental investigations have been performed in order to clarify the properties of Al and P impurities in both crystalline and amorphous silica,[1–11] but the experimental techniques employed usually only yield indirect information about the geometry and electronic structure of the impurities and their local environments. Thus there is a need to complement the experimental investigations by theoretical studies that may provide a link between the ''fundamental'' impurity properties and the experimentally accessible quantities (e.g., results from optical or magnetic resonance spectroscopies). Two theoretical techniques have in recent years proven succesful for investigations of defects and impurities in silica. One approach[12–17] is based on traditional quantum-chemical methods using cluster models and a basis set consisting of local orbitals (usually Gaussians), and a variety of energy functionals such as Hartree-Fock, second-order Moller-Plesset (MP2), and various approximations to density functional theory (DFT).[18–20] The other [21–29] is based on repeated supercell models and DFT energy functionals, which are in most cases evaluated using a plane-wave representation of the Kohn-Sham wave functions and non- or semilocal pseudopotentials to describe the electronic states close to the nuclei in an efficient manner. We have recently presented a study of implanted and substitutional Al and P impurities in silica using a DFT-based supercell method.[29] The purpose of the present work is to extend the study of the substitutional impurities through a calculation of the hyperfine matrices for the magnetic nuclei ^{27}Al, ^{29}Si, ^{31}P, and ^{17}O.

Several theoretical studies of substitutional Al impurities have been reported earlier,[12,13,27–29] but the results from Hartree-Fock cluster calculations[12,13] have not been consistent with those of DFT-based supercell approaches.[27–29] Recently, two independent works have compared results of cluster calculations using a DFT-like functional to those obtained with the Hartree-Fock method[30,31] and in one case also the MP2 functional.[30] The DFT geometries were similar to those obtained in supercells, and the hyperfine parameters were in clear disagreement with experimental results, indicating that the choice of an energy functional free of self-interaction is decisive for describing the physics of this system correctly. In the present paper we show that, while the supercell DFT calculations for the substitutional Al impurity as expected yields hyperfine parameters in strong disagreement with experiment, the method accounts well for the hyperfine parameters of substitutional P. Thus, the DFT is appropriate for describing the behavior of a single electron in the silica conduction bands, but fails in the description of a single hole in the valence band. It is argued that this is partly due to the different nature of the silica valence and conduction bands and partly to the DFT self-interaction error being larger for holes than for electrons.

The remainder of the paper is organized as follows: In Sec. II we briefly review the calculation of hyperfine matrices within the framework of ultrasoft pseudopotential (US-PP) theory. In Sec. III our numerical results are presented and discussed, while Sec. IV summarizes our conclusions.

II. THEORETICAL APPROACH

When evaluating hyperfine matrices it is important to describe the wave function correctly close to the nuclei, which

is difficult within traditional norm-conserving pseudopotential approaches. It has recently been shown,[32] however, that the ultrasoft pseudopotential (US-PP) scheme originally introduced by Vanderbilt[33] can be viewed as an approximation to the projector-augmented-wave (PAW) all-electron method developed by Blöchl.[34] In this method the wave function is expanded in a basis of plane waves augmented by atomic orbitals inside spheres centered around the ions on the lattice:

$$\Psi_{n\mathbf{k}\sigma}=\tilde{\Psi}_{n\mathbf{k}\sigma}+\sum_i \langle\tilde{\Psi}_{n\mathbf{k}\sigma}|\beta_i\rangle(\phi_i-\tilde{\phi}_i). \tag{1}$$

Here σ is a spin index, which we, for convenience, shall take to assume the values ± 1. The functions ϕ_i and $\tilde{\phi}_i$ are atomic orbitals (i.e., a radial function times a spherical harmonic) centered on a particular site in the crystal, and are chosen to be identical outside the augmentation spheres, implying that $\Psi_{n\mathbf{k}\sigma}$ and $\tilde{\Psi}_{n\mathbf{k}\sigma}$ are also identical in this region. i is to be understood as a combined orbital, spin, and site index. The ϕ_i functions are solutions of the all-electron Kohn-Sham equations[19] in the free atom, at chosen energies (usually the atomic eigenvalues are included), while the $\tilde{\phi}_i$ are soft pseudo-orbitals. The functions β_i are a set of duals to the pseudo-orbitals, i.e.,

$$\langle\beta_j|\tilde{\phi}_i\rangle=\delta_{ij}\,. \tag{2}$$

Under the assumption of ''pseudocompleteness,'' by which we shall understand fulfillment of the requirement

$$\tilde{\Psi}_{n\mathbf{k}\sigma}=\sum_i \langle\tilde{\Psi}_{n\mathbf{k}\sigma}|\beta_i\rangle\tilde{\phi}_i \tag{3}$$

and thereby

$$\Psi_{n\mathbf{k}\sigma}=\sum_i \langle\tilde{\Psi}_{n\mathbf{k}\sigma}|\beta_i\rangle\phi_i \tag{4}$$

within the augmentation spheres, the charge density may be written as[34]

$$n(\mathbf{r},\sigma)=\sum_{n\mathbf{k}\sigma} f(\varepsilon_{n\mathbf{k}\sigma}-\mu_c)\{|\tilde{\Psi}_{n\mathbf{k}\sigma}(\mathbf{r})|^2+\sum_{ij}\langle\tilde{\Psi}_{n\mathbf{k}\sigma}|\beta_i\rangle \times\langle\beta_j|\tilde{\Psi}_{n\mathbf{k}\sigma}\rangle Q_{ij}(\mathbf{r}-\tau_i)\}, \tag{5}$$

$$Q_{ij}(\mathbf{r})=\phi_i^*(\mathbf{r})\phi_j(\mathbf{r})-\tilde{\phi}_i^*(\mathbf{r})\tilde{\phi}_j(\mathbf{r}). \tag{6}$$

$\boldsymbol{\tau}_i$ is the position vector of the augmentation sphere containing orbital i (we assume nonoverlapping spheres so that the ij sum can be restricted to orbital pairs belonging to the same sphere). f is the Fermi function and μ_c the chemical potential. Usually only *spd* orbitals are included in the $\phi_i\,,\tilde{\phi}_i$ basis set.

In both the PAW and US-PP methods it is convenient to introduce smooth pseudodensities, $\tilde{n}$ and $\tilde{n}_{\mathrm{aug}}$, given by

$$\tilde{n}(\mathbf{r},\sigma)=\sum_{n\mathbf{k}\sigma} f(\varepsilon_{n\mathbf{k}\sigma}-\mu_c)|\tilde{\Psi}_{n\mathbf{k}\sigma}(\mathbf{r})|^2, \tag{7}$$

$$\tilde{n}_{\mathrm{aug}}(\mathbf{r},\sigma)=\tilde{n}(\mathbf{r},\sigma)+\sum_{n\mathbf{k}\sigma} f(\varepsilon_{n\mathbf{k}\sigma}-\mu_c)\sum_{ij}\langle\tilde{\Psi}_{n\mathbf{k}\sigma}|\beta_i\rangle \times\langle\beta_j|\tilde{\Psi}_{n\mathbf{k}\sigma}\rangle\tilde{Q}_{ij}(\mathbf{r}-\tau_i). \tag{8}$$

$\tilde{Q}_{ij}$ is a set of pseudoaugmentation charges, determined so as to preserve the lowest moments of the Q_{ij}'s. In this way, the long-range electrostatic interactions are correctly described by the pseudo-charge-density, and the pseudo-Hartree and exchange-correlation (xc) energy terms need only be corrected inside the atomic spheres. This is conveniently done by a nonlocal potential term.[34,33] In the PAW method the correction is exact, so in this approach the DFT energy functional corresponding to the density in Eq. (5) is minimized with the pseudo-wave-functions $\tilde{\Psi}_{n\mathbf{k}\sigma}$ as variational parameters. In the US-PP method the correction is approximate, based on a linearization around the free-atom occupancies.[32] In practice, the two methods yield results in good agreement with each other. Assuming that the US-PP $\tilde{\Psi}_{n\mathbf{k}\sigma}$ is not too different from the corresponding PAW quantity, it follows that a good approximation to the all-electron wave function may be constructed on the basis of a US-PP calculation by use of Eq. (1). In the context of calculating hyperfine parameters this approach was originally introduced by Van de Walle and Blöchl,[35] and we shall proceed along similar lines.

The interaction between an unpaired electron spin and a magnetic nucleus can formally be written as

$$\hat{\mathbf{I}}\cdot\overline{\overline{A}}\cdot\hat{\mathbf{S}}. \tag{9}$$

Here $\hat{\mathbf{I}}$ and $\hat{\mathbf{S}}$ are the quantum-mechanical (vector) operators for the nuclear and electronic spins, respectively, while $\overline{\overline{A}}$ is the hyperfine matrix. This may in turn be evaluated from the electronic spin density as

$$\overline{\overline{A}}=A_{\mathrm{iso}}\overline{\overline{I}}+\overline{\overline{A}}_{\mathrm{an}}, \tag{10}$$

$$A_{\mathrm{iso}}=\frac{2}{3}\mu_0\beta_e\beta_I n_{\mathrm{spin}}(0), \tag{11}$$

$$A_{\mathrm{an}}^{\mu\nu}=\frac{\mu_0}{4\pi}\beta_e\beta_I\int d\mathbf{r}\, n_{\mathrm{spin}}(\mathbf{r})\frac{3x^\mu x^\nu-\delta_{\mu\nu}r^2}{r^5}, \tag{12}$$

taking the nucleus to be at the origin of coordinates. Here μ_0 is the vacuum permeability, while β_e and β_I are the magnetic moments of the electron and nucleus, respectively. n_{spin} is the electronic spin density and $\overline{\overline{I}}$ the unit matrix. Using the augmented pseudodensity, $\tilde{n}_{\mathrm{aug}}(\mathbf{r},\sigma)$ given by Eq. (8), and its Fourier transform $\tilde{n}_{\mathrm{aug}}(\mathbf{G},\sigma)$, it is a straightforward exercise to show that

$$n_{\mathrm{spin}}(0)=\sum_\sigma \sigma\tilde{n}(0,\sigma)+\sum_{n\mathbf{k}\sigma} f(\varepsilon_{n\mathbf{k}\sigma}-\mu_c)\sum_{ij}\sigma\langle\tilde{\Psi}_{n\mathbf{k}\sigma}|\beta_i\rangle \times\langle\beta_j|\tilde{\Psi}_{n\mathbf{k}\sigma}\rangle Q_{ij}(0), \tag{13}$$

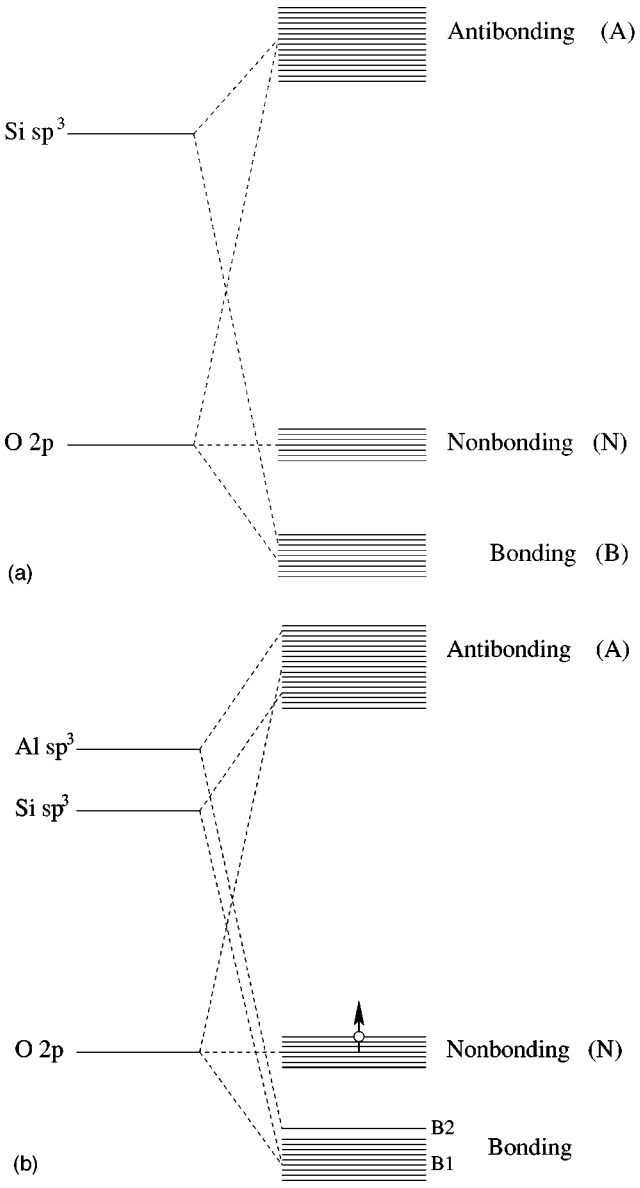

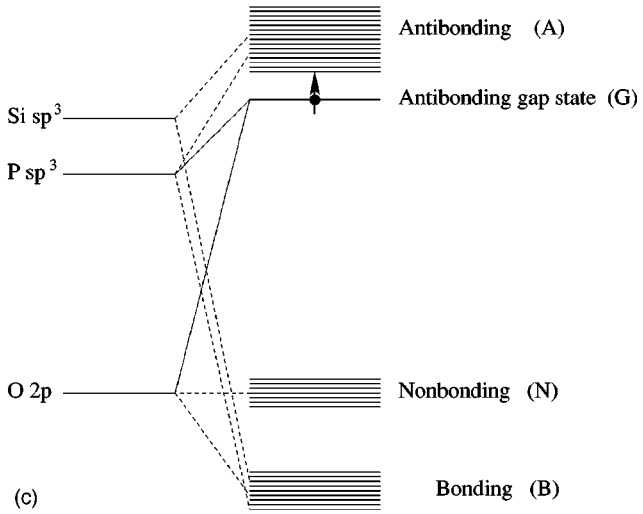

FIG. 1. Simplified level schemes for substitutional impurities in silica. In (a), a level diagram for pure silica is shown: The Si $3sp$ levels hybridize to the O $2p$ levels to form occupied bonding, and unoccupied antibonding states, separated by a set of occupied nonbonding orbitals derived from O $2p$ states. In (b) the levels at an Al impurity site are depicted: The Al level leads to new bonding states (B2), and antibonding states buried in the conduction bands. An unpaired hole is present in the top of the valence bands. In (c) we show the corresponding levels at a P impurity. Here, the lower position of the P $3sp$ levels compared to those of Si gives rise to a gap level holding an unpaired electron. The P-O bonding states are situated at the bottom of the Si-O bonding-state bands.

$$\int d\mathbf{r}\, n_{\mathrm{spin}}(\mathbf{r})\frac{3x^{\mu}x^{\nu}-\delta_{\mu\nu}r^2}{r^5}$$
$$=\sum_{\sigma}\sigma\Bigg\{\sum_{\mathbf{G}\neq\mathbf{0}}\frac{4\pi}{3}\tilde{n}_{\mathrm{aug}}(\mathbf{G},\sigma)\frac{3G^{\mu}G^{\nu}-\delta_{\mu\nu}G^2}{G^2}$$
$$+\sum_{n\mathbf{k}} f(\varepsilon_{n\mathbf{k}\sigma}-\mu_c)\sum_{ij}\langle\tilde{\Psi}_{n\mathbf{k}\sigma}|\beta_i\rangle\langle\beta_j|\tilde{\Psi}_{n\mathbf{k}\sigma}\rangle$$
$$\times\int_0^{r_c}d\mathbf{r}[Q_{ij}(\mathbf{r})-\tilde{Q}_{ij}(\mathbf{r})]\frac{3x^{\mu}x^{\nu}-\delta_{\mu\nu}r^2}{r^5}\Bigg\}. \qquad (14)$$

A similar result was recently reported by Blöchl.[36] Notice that since $\tilde{n}_{\mathrm{aug}}$ correctly reproduces the multipole moments of n in the neighboring spheres we only need to include augmentation corrections in the sphere containing the magnetically active nucleus.

These formulas summarize the contribution to the hyperfine matrix from the valence electrons. The presence of a nonzero valence electron spin density will modify the shape of the core wave functions and create an additional contribution to the spin density at the nucleus, which in some cases can be important. To account for this effect, we solve the radial Schrödinger equation for the core states, treating the spherically averaged spin-dependent contribution to the Kohn-Sham potential from the valence electron density as a fixed external potential. Nonspherical perturbations of the core states are neglected, and the spin polarization of the core states therefore only affects the isotropic part of the hyperfine matrix.

III. NUMERICAL RESULTS AND DISCUSSION

We have previously calculated the electronic and geometric structure of substitutional Al and P impurities in silica,[29] and the present investigation is based on these results. The

TABLE I. Principal values of the ^{31}P hyperfine tensor (in mT) for different P pseudopotentials. PP1 has two atomic orbitals in each of the *sp* channels and one in the *d* channel; PP2, PP3, and PP4 have an extra orbital in the *s*, *p*, and *d* channels, respectively.

	A_{iso}	A_{an} principal values		
PP1	140.8	9.77	-4.55	-5.23
PP2	140.8	9.77	-4.55	-5.23
PP3	142.8	9.66	-4.52	-5.13
PP4	141.8	9.76	-4.54	-5.22
Expt. (Ref. 3)	112.9	9.91	-4.36	-5.54

essence of the electronic structures found is summarized in Fig. 1. In pure silica, the top of the valence band is formed by a set of nonbonding O states, lying above the Si-O bonding states. The conduction band is formed by antibonding Si-O states. As the Al 3*sp* levels lie slightly above the Si ones, the Al-O bonding states of a substitutional Al impurity will appear in the gap between bonding Si-O and nonbonding O states, whereas the Al-O antibonding states will be buried in the Si-O conduction bands. Al has one electron less than Si, so a hole will be present in the top of the valence band, that is, in the nonbonding O bands. In the case of substitutional P, on the other hand, the impurity 3*sp* levels lie below those of Si, so the bonding P-O states appears at the lower edge of the Si-O ones, while the antibonding states falls below the conduction band and forms a gap state. One spin channel of this gap state is occupied, since P has one electron more than Si. Thus, the hole introduced by Al substitution moves in an orbital space that is quite different from that which is accessible to the electron introduced by P substitution, a fact that will be shown to have important consequences for the reliability of the DFT approach.

A. ^{31}P hyperfine parameters

To investigate the accuracy of the pseudopotential approach to calculation of hyperfine parameters described above, ^{31}P hyperfine matrices were calculated using P pseudopotentials with a different number of augmentation orbitals in the various angular-momentum shells. The results are shown in Table I. It can be seen that the uncertainties associated with the atomic orbital basis set are on the order of 1%, which is less than the errors commonly encountered when comparing theoretical values of hyperfine matrices to experiment. The present calculation gives a good reproduction of the anisotropic part of the hyperfine matrix, whereas the isotropic part is ~25% off. It is well known from other studies that the isotropic term is the most difficult to reproduce,[35] presumably because of the approximate description of relativistic and exchange-correlation effects close to the nucleus. Core polarization effects were found to add about 1% to the total isotropic shift in this case. The high accuracy of the calculated anisotropic terms suggests that it is only the wave function very close to the nucleus that is inadequately described by the present theory. The principal directions of the hyperfine matrix (calculated with the pseudopotential labeled PP1 in Table I) are compared to the experimentally determined ones in Table II. The variation of these directions between the different pseudopotentials was found to be on the order of 1%. Again, the agreement between theory and experiment is quite good, apart from an interchange of two eigenvectors. Uchida and co-workers[3] found the eigenvector of the lowest eigenvalue to lie approximately along the line connecting the two oxygen atoms, which would be short-bonded to the substitutional P if no structural relaxations occurred compared to pure silica. However, in our calculation we find that the order of long and short bonds is interchanged around P, i.e., the short-bonded O atoms around an Si atom become the long-bonded O atoms around the substitutional P impurity. Thus, while the conclusion of Uchida *et al.* that the lowest eigenvalue is in the direction of the short bonds is upheld, this direction is changed relative to the crystal axes by the structural relaxations. As the difference between long and short bonds in α-quartz is very small (~0.004 Å), the most likely explanation of the discrepancy, compared to experiment, in the eigenvector ordering then seems to be that the calculation for some reason (perhaps the finite size of the supercell) erroneously interchanges the order of long and short bonds.

TABLE II. Principal directions for the eigenvectors of the ^{31}P hyperfine tensor in spherical polar coordinates. θ measures the angle between the vector $\mathbf{P}_i$ and the *c* direction, while ϕ measures the rotation with respect to one of the C_2 symmetry axes of the crystal. The vectors are ordered according to decreasing principal values.

	Theory		Experiment (Ref. 3)	
	θ (deg)	ϕ (deg)	θ (deg)	ϕ (deg)
$\mathbf{P}_1$	90.0	0.0	90.0	0.0
$\mathbf{P}_2$	30.0	270	64.8	90.0
$\mathbf{P}_3$	60.0	90	25.2	270

TABLE III. Principal values of the ^{17}O and ^{29}Si hyperfine tensors (in mT) for the nearest O and Si neighbors of a substitutional P impurity. O(1) are the long-bonded (to P) O neighbors, and O(2) the short-bonded ones. Si(1) and Si(2) are neighbors of O(1) and O(2), respectively.

	A_{iso}	A_{an} principal values		
O(1)	-8.47	1.28	1.19	-2.36
O(2)	-1.73	0.28	0.26	-0.54
Si(1)	-1.80	0.14	0.14	-0.28
Si(2)	-0.37	0.03	0.01	-0.04

In Table III the predicted hyperfine parameters for the Si and O atoms closest to P are listed. It can be seen that a substantial part of the unpaired spin is found on the O atoms that have the longer bonds to P, while the spin density is much reduced on the short-bonded O atoms in accordance with the analysis of the density of states (DOS) presented in Ref. 29. Core polarization effects were found to increase the isotropic coupling constant by ~1% for Si and decrease it by ~4% for O. No experimental values for the ^{17}O hyperfine matrices have, to our knowledge, been reported. The

spin density on the neighboring Si atoms is very small, as can be inferred from the smallness of the hyperfine parameters. In fact, even for the Si atoms neighboring the long-bonded (to P) O atoms, the integrated spin density within the Si augmentation spheres, as estimated using Eq. (4), corresponds to only 0.015 electrons. Experimentally, a hyperfine doublet with a splitting of 0.16 mT with the magnetic field in the *z* direction was assigned to interactions with ^{29}Si nuclei, suggesting that the present calculation does not provide an accurate description of very small spin concentrations. Similar problems have been reported by Van de Walle and Blöchl.[35] In conclusion, the supercell DFT calculation seems to provide a fairly accurate description of the electronic structure around a substitutional P impurity.

B. Hyperfine parameters around an Al impurity

The unpaired spin state around the substitutional Al impurity is situated at the top of the valence band, that is, in the O nonbonding states. Put in another way, the hole introduced on Al is transferred to one or more neighboring O atoms. There is abundant evidence from EPR experiments on irradiated α-quartz crystals that the spin is in fact localized on one of the long-bonded O neighbors: Signals from six different *g*-tensor orientations can be discerned in EPR spectra, corresponding to holes sitting at each of the two long-bonded O neighbors to the three symmetry-equivalent Al positions available.[37,38] Cross-relaxation experiments and dielectric loss measurements have indicated that the hole may hop back and forth between the two long-bonded O atoms.[39] The apparent confinement of the unpaired spin on one of two symmetry-related O atoms indicates a dynamical localization effect: The presence of the hole on one of the equivalent O neighbors creates a polarization ''cloud'' in the surrounding lattice, and this cloud impedes hole hopping between O atoms.[40] Thus, in the theoretical calculations we should expect to see either a preference for structural distortions creating a localized hole state, or at least a tendency for the hole to localize quickly if a distortion is enforced. However, we have not observed any of these effects in the supercell calculations. On the contrary, if the structure is allowed to fully relax, the Al-O bonds end up being pairwise equivalent, and with very small differences in bond length between pairs.[29] This structure is stable towards distortions. A similar result was found by Magagnini *et al.* using the local spin density approximation (LSDA).[28] The spin densities on the short- and long-bonded O atoms differ by less than 10%. If a structural distortion is enforced, only a slow variation in the spin densities is seen, and the energy penalty quickly rises. That the spin distribution associated with the theoretical optimum geometry is not consistent with the experimental results for ^{17}O hyperfine matrices[41] can be seen at a glance from Table IV. Given the accuracy of the theoretical ^{31}P hyperfine parameters reported above and the large spin population on the O atoms, it is unlikely that the large deviations from experiment are merely caused by basis set inaccuracies. It must be concluded that the spin density distribution found by the supercell method in conjunction with DFT is incorrect, and that the picture of this impurity state put forward in Refs. 28 and 29 is thereby invalidated.

TABLE IV. Isotropic and anisotropic contributions to the hyperfine coupling tensors around a neutral substitutional Al impurity (in mT), as calculated using the PW91 energy functional in a 54-atom repeated-cell geometry.

	A_{iso}	A_{an} principal values		
^{27}Al theory	-1.018	0.010	-0.001	-0.010
^{27}Al expt. (Ref. 41)	-0.578	0.074	-0.034	-0.034
^{17}O(1) theory	-1.372	1.145	1.117	-2.262
^{17}O(2) theory	-1.601	1.271	1.242	-2.513
^{17}O expt. (Ref. 41)	-2.594	4.382	4.121	-8.504

To clarify the reason for these inaccuracies a new investigation of the substitutional Al impurity within the cluster approximation was performed. The calculations were performed using either the Hartree-Fock energy functional or the hybrid Hartree-Fock–DFT functional B3LYP proposed by Becke,[42] which has proven highly accurate for a variety of chemical systems. The calculational procedures and some of the results were presented in Ref. 31, and similar work has independently been reported by Pacchioni *et al.*[30] It was found that there is a qualitative difference between the results of the two energy functionals considered: While the Hartree-Fock approximation favors a structural distortion with one Al-O bond becoming $\sim$14% longer than the other three, the B3LYP energy functional does not lead to such a distortion but rather to a restoration of the C_2 symmetry of the cluster, which was explicitly broken in the initial configuration. The bond lengths obtained in this calculation are close to the supercell Perdew-Wang 1991 (PW91) result.[43] The differences in structure are reflected in the Mulliken populations: Using the B3LYP functional, spin densities resembling those arising in the supercell calculations are obtained, while in the Hartree-Fock case, the unpaired spin is almost completely localized on the long-bonded O atom. These results indicate that the removal of the periodic Al images has no significant effect on the electronic structure of the impurity, whereas the choice of an energy functional (Hartree-Fock) with exact self-interaction cancellation is decisive in obtaining agreement with the experimental picture.

The calculated hyperfine parameters are reported in Table V. The results obtained within the Hartree-Fock approximation are in good agreement with the experimental values, especially for the anisotropic tensor, while the B3LYP results are closer to those obtained in the supercell PW91 calculation, and in clear disagreement with experiment. In the Hartree-Fock equilibrium geometry both energy functionals have been applied, and it can be seen that the Hartree-Fock approximation still provides the best description of the anisotropic couplings, although the B3LYP results are not too far from the experimental values in this case. For the isotropic ^{17}O coupling constant the situation is reversed: Here, the B3LYP approximation provides the better description. In our view, this improvement is most likely to be accidential: While the anisotropic hyperfine tensor is roughly proportional to the O $2p$ weight of the hole wave function on the O atom in question, the isotropic coupling is only dependent on the *s* component, which is very small. Furthermore, the iso-

TABLE V. Isotropic and anisotropic contributions to the hyperfine coupling tensors around a neutral substitutional Al impurity (in mT), as calculated using the Hartree-Fock and B3LYP energy functionals in an $AlSi_{16}O_{16}H_{36}$ cluster geometry. The results denoted HF-B3LYP were calculated in the Hartree-Fock equilibrium geometry using the B3LYP energy functional. In all cases, O(1) denotes the O neighbor with the longest bond to Al.

	A_{iso}	A_{an} principal values		
^{27}Al Hartree-Fock	-0.587	0.066	-0.032	-0.034
^{27}Al HF-B3LYP	-0.498	0.062	-0.024	-0.038
^{27}Al B3LYP	-0.791	0.028	-0.002	-0.025
^{27}Al expt. (Ref. 41)	-0.578	0.075	-0.034	-0.035
^{17}O(1) Hartree-Fock	-4.247	4.475	4.461	-8.935
^{17}O(1) HF-B3LYP	-2.231	3.617	3.605	-7.221
^{17}O(1) B3LYP	-0.548	0.924	0.910	-1.834
^{17}O expt. (Ref. 41)	-2.594	4.382	4.121	-8.504

tropic coupling is only determined by the wave function very close to the nucleus, which is difficult to describe using a Gaussian basis set, and where relativistic effects not accounted for in the calculation may lead to further inaccuracies. Therefore, the calculation of the isotropic coupling constant is more prone to technical errors than the anisotropic tensor, as was also evident in the supercell results for substitutional P.

To investigate the implications of the spurious self-interaction on the total energy some additional calculations have been performed, the results of which are summarized in Table VI. First, we have calculated the energy difference between the HF and B3LYP equilibrium geometries within each of the two approximations. To focus attention on the effect of relaxations around the Al ion, we have subtracted the energy difference between HF and B3LYP equilibrium geometries for a pure neutral SiO_2 cluster. With this correction, the penalty within B3LYP for going from the B3LYP to the HF equlibrium geometry is 0.15 eV, whereas the penalty within HF for going the other way is 2.23 eV. Since the results for the hyperfine matrices show that the true equilibrium geometry must be close to the HF geometry, this indicates that the magnitude of the B3LYP error is at least on the order of 0.2 eV. However, the large energy difference within the HF approximation suggests that the error could be much more severe.

To shed more light on this question we have also calculated the charging energy of the impurity cluster within the two approximations. In contrast to the neutral cluster, only small differences between unrestricted HF and B3LYP equilibrium geometries are found in this case. In both approximations, the cluster goes into a C_2 symmetric configuration, as would be expected with all valence bands filled up. The Al-O equilibrium bond lengths are 1.727 Å and 1.741 Å in the HF versus 1.742 Å and 1.756 Å in the B3LYP geometries. We find the negatively charged cluster to be stable in both approximations, with a trapping energy (i.e., the difference between total energies in the charged and neutral relaxed configurations) of 5.29 eV in HF and 6.33 eV in the B3LYP approximation. Note that these energies represent trapping from the vacuum into a small cluster, and may be substantially different from the trapping energies for electrons trapped from the conduction band of an extended solid. Assuming that the B3LYP method describes the charged configuration correctly, we should expect the B3LYP trapping energy to be too high, as the method fails to capture the energy gain from the structural relaxation in the neutral cluster. On the other hand, the HF trapping energy is probably too low, as electron correlations, which are left out of the HF approximation, are usually more important in negatively charged systems. For instance, Pacchioni and Mazzeo[44] found a difference in trapping potential of ~ 1.5 eV between the HF and B3LYP approximations for a substitutional Ge impurity in silica using computational methods similar to ours. Also in this case, the B3LYP approximation provided the deeper potential, although there was no qualitative difference in the atomic geometries between the different approximations. Thus, the result for the charging energy place a more stringent upper bound of around 1 eV on the total-energy error arising from the wrong B3LYP geometry, and it seems likely that the error is, in fact, somewhat smaller than this.

C. Discussion: Validity of the PW91 and related approaches

The results presented above show that the PW91 approximation adequately describes the electronic structure of a neutral substitutional P impurity in α-quartz but fails dramatically for the corresponding Al impurity. In the present case, both impurities have been reliably identified and their EPR properties have been characterized in great detail. This is not, however, generally the case for impurity states in silica, or other materials for that matter, and an important role of an impurity theory is to provide reliable information that may aid the identification of various impurities from the available experimental information (usually from optical or magnetic resonance spectroscopies). As the DFT in most cases constitutes an improvement over Hartree-Fock theory, it is impor-

TABLE VI. Total energies (in hartree units) of the cluster configurations investigated. B3LYP/HF denotes a B3LYP calculation in a Hartree-Fock equilibrium geometry, etc.

	Neutral SiO_2	Neutral SiO_2:Al	Charged SiO_2:Al
B3LYP/B3LYP	-6147.8842	-6100.7166	-6100.9493
B3LYP/HF	-6147.8690	-6100.6962	-
HF/B3LYP	-6131.7217	-6084.5123	-
HF/HF	-6131.7227	-6084.5954	-6084.7897

tant to clarify the reasons for its failure in the present case, in order to determine when this theoretical approach can and cannot be applied.

1. Localization barriers for holes and electrons

The main chemical difference between the substitutional Al and P impurities is that Al donates a hole to the top of the SiO_2 valence band, while P donates an electron to the bottom of the conduction band. These two bands are, however, of a quite different nature, as seen from Fig. 1. The top of the valence bands consists of O $2p$ nonbonding states, while the bottom of the conduction bands is made up of Si-O antibonding orbitals. Thus, the injected hole will move in a space of weakly coupled (as they do not point towards each other), nearly degenerate O $2p$ orbitals surrounding the Al impurity (to which the hole is bound for electrostatic reasons), while the injected electron will move in a space consisting of the P $3sp$ hybrid orbitals and the O $2p$ orbitals pointing towards the P atom. These orbitals have strong overlaps, meaning that the effective Hamiltonian for the electron is not sensitive to a small residual self-interaction in the DFT energy functional. For the hole moving in the nonbonding O $2p$ orbitals, on the other hand, even a small residual self-interaction may outweigh the O $2p$ level differences caused by structural distortions, thus preventing the hole from localizing on the orbital of highest energy, which in turn makes the distortion less favorable.

To formalize the argument, we set up a minimal model for the hole energy functional in the different approximations. Focusing attention on the electrons in the minority spin channel that need to be accommodated in the nonbonding O $2p$ orbitals surrounding the Al impurity, we assume that the interaction with the other electrons in the system may be well represented by suitably chosen orbital energies, and that the coupling to other orbitals is sufficiently weak that these do not need to be incorporated in the basis. Furthermore, we neglect the overlap between the different O $2p$ orbitals to keep the effective Hamiltonian simple, although it should be kept in mind that a small overlap does in fact exist. The total-energy functional may then be written as[31]

$$E = C + \sum_i \varepsilon_i \rho_{ii} + \frac{1}{2} \sum_{ij} U_{ij} \rho_{ii} \rho_{jj} + E_{\mathrm{xc}}[\rho], \qquad (15)$$

where ρ is the density matrix of the minority spin electrons, and i,j indexes the nonbonding O $2p$ states on different sites. ε_i collects all terms linear in ρ except those arising from the xc energy, and C denotes the ρ-independent terms. The U_{ij} parameters are the Coulomb integrals between $2p$ charge distributions on sites i and j. The different total-energy approximations are distinguished by different choices of E_{xc}. In the HF approach the exact exchange energy is the only contribution retained, while in DFT the xc energy is usually a complicated local functional of the total electron density and possibly its gradient. Thus, we may write

$$E_{\mathrm{xc}}^{\mathrm{UHF}}[\rho] = -\frac{1}{2} \sum_{ij} \rho_{ij} \rho_{ji} U_{ij}, \quad E_{\mathrm{xc}}^{\mathrm{DFT}}[\rho] = \sum_i E_{\mathrm{loc}}(\rho_{ii}), \qquad (16)$$

assuming that there is no difference between the form of the basis orbitals on the different O sites in question.

In the HF approximation, as is well known, the present case of a single hole moving in a filled band is formally equivalent to that of a single electron moving in an empty band, and both cases are free of self-interaction, as one can easily verify from Eqs. (15) and (16). In DFT, both the explicit self-interaction cancellation and the electron-hole symmetry is lost. For the approximate xc functionals commonly employed, it has been found that the Hartree part of the self-interaction dominates the xc part such that an unphysical localization barrier is present. Considering the energy functional in Eq. (15) with N equivalent orbitals, we can define the localization barrier as the energy difference between the case of a particle (electron or hole) localized on a single orbital and one that is evenly distributed over all orbitals:

$$E_{\mathrm{loc}}^{e} - E_{\mathrm{deloc}}^{e} \equiv \delta_N^e. \qquad (17)$$

For large N, the result is well known:[45]

$$\delta_\infty^e = \frac{U}{2} + E_{\mathrm{loc}}(1). \qquad (18)$$

Since E_{deloc} goes to zero for an extended state, δ_∞^e represents an upper limit on the localization barrier. Note that δ_∞^e is entirely specified by the shape of the local orbital and the xc functional used. Typical values for real atomic orbitals are on the order of 0.1–1 eV.[45,46] For a hole, one derives the general result [for a local xc functional as in Eq. (16)]:

$$\delta_N^h - \delta_N^e = (N-2) E_{\mathrm{loc}}(1) + N\left[E_{\mathrm{loc}}\left(\frac{1}{N}\right) - E_{\mathrm{loc}}\left(1 - \frac{1}{N}\right)\right]. \qquad (19)$$

The individual values of δ_N^e and δ_N^h cannot be estimated without making assumptions about the atomic geometry due to the long-range part of the Hartree interaction. The above formula reflects the fact that the Hartree energy functional preserves electron-hole symmetry so that the difference between hole and electron localization energies is entirely determined by the xc terms. In the large-N limit one derives[31]

$$\delta_\infty^h = \langle \hat{V}_H + \hat{V}_{\mathrm{xc}} \rangle - \delta_\infty^e, \qquad (20)$$

$\hat{V}_H$ and $\hat{V}_{\mathrm{xc}}$ being the Hartree and xc potential operators, and the expectation value being over a single orbital. The expectation value of the potentials can be an order of magnitude larger than δ_∞^e.[45–47] However, in a typical impurity problem, the hole is restricted to move in a finite number of orbitals, and it is therefore important to investigate the behavior of Eq. (19) for this situation. To this end, we have performed a local spin density (LSD) calculation for a neutral isolated O atom. The functional E_{loc} appearing in Eq. (19) is then obtained by evaluating the LSD energy functional on the resulting self-consistent O $2p$ orbital (assuming a fully spin-polarized density). The result for $\delta_N^h - \delta_N^e$ is shown in Fig. 2. Of course, this should only be considered a rough estimate of the actual localization barrier, as interactions with other orbitals and relaxation effects upon changes

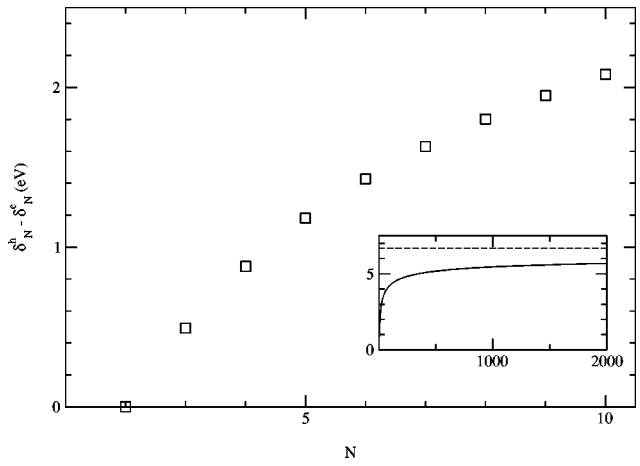

FIG. 2. The difference between hole and electron localization barriers as a function of the orbital degeneracy evaluated using an LSD energy functional on a self-consistent O $2p$ orbital from an atomic calculation. The inset shows the behavior for a large number of orbitals. Note that the asymptotic result (dashed line in inset) is approached very slowly.

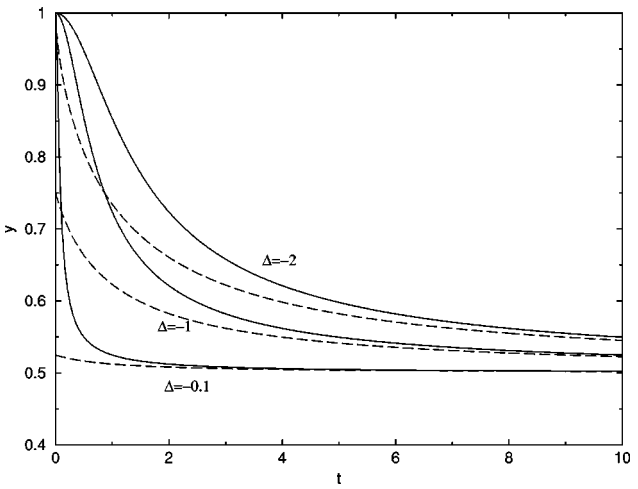

FIG. 3. Optimum y parameters at $U=0$ (solid lines) and $U=1$ (dashed lines) as a function of t for different values of Δ. The parameters are defined in the text.

in occupancy have been neglected. Still, it is interesting to notice, that whereas δ^e_∞ comes out as ~ 0.27 eV, the difference between the hole and electron barriers is on the order of an eV, even for small N. On the other hand, the asymptotic limit (indicated by a dashed line in the inset) is approached very slowly. This means that Eq. (20) does not necessarily constitute a good starting point for deriving realistic self-interaction corrected hole energy functionals within the framework of DFT.

2. Validity of models with self-interaction

To shed more light on the importance of residual self-interactions in various physical problems we shall investigate their consequences for different level separations and hopping integrals in a very simplified model: Consider a single particle (in this case an electron) moving in a space of two orbitals, with an energy separation of Δ and a hopping parameter t. Introducing the density matrix of the electron ρ_{ij} (for $i,j \in \{1,2\}$) we write the energy functional as

$$E = \Delta\rho_{11} + 2t\rho_{12} + U(\rho_{11}^2 + \rho_{22}^2). \tag{21}$$

U thus represents the residual self-interaction present in the model. The density matrix may be expressed in terms of a single parameter,

$$\rho_{11} = y, \quad \rho_{22} = 1-y, \quad \rho_{12} = -\mathrm{sgn}(t)\sqrt{y(1-y)}, \tag{22}$$

and the energy functional can thus be written

$$E = \Delta y - 2|t|\sqrt{y(1-y)} + U(2y^2 - 2y + 1). \tag{23}$$

In Fig. 3 we show the values of y minimizing the energy for $U=1$ and $U=0$ (no self-interaction). The results are plotted as a function of t for various values of Δ. It can be seen that the self-interaction term is of limited consequence as long as it is a few times or more smaller than Δ or t, whereas serious discrepancies develop if U dominates the other parameters. Thus, to assess the validity of DFT methods in a single-particle-like problem one must estimate the magnitude of the DFT self-interaction and compare it to the level differences and hopping matrix elements of the relevant orbitals. In the present cases, the hole bound to the substitutional Al impurity is moving in a space of nonbonding O $2p$ orbitals. The hopping matrix element between these states was estimated to be ~ 0.06 eV in Ref. 31. In comparison, the hole localization barrier resulting from unphysical self-interactions was estimated above to be on the order of 1 eV, an order of magnitude larger than the hopping matrix element. In this regime, serious discrepancies due to self-interaction errors can be expected, as is clearly seen from Fig. 3. For the electron bound to the substitutional P impurity the situation is very different: This electron primarily moves in the space of antibonding P-O orbitals and is found to localize in one pair of these through a lattice distortion. The self-interaction for an *electron* in these states must be expected to be much lower than the 0.27 eV estimated for an O $2p$ state since the antibonding P-O states are more extended. The hopping matrix elements between the states can be estimated from the matrix element between the phosporous sp^3 hybrids, which is given by $\approx \frac{1}{4}(\varepsilon_s - \varepsilon_p) \sim -2$ eV.[48] The P-O antibonding states have most of their weight on the P atom, and thus a hopping matrix element of magnitude 1–2 eV. This estimate is in good agreement with the splitting of ~ 3 eV between occupied and unoccupied antibonding states seen in Fig. 1(b) of Ref. 29. Therefore, in the case of substitutional P, the hopping terms of the effective Hamiltonian for the unpaired spin are at least 4 times larger than the unphysical localization barrier. It is evident from Fig. 3 that this will not cause major inaccuracies in the resulting electron distribution.

3. The eigenvalue spectrum

The remarkable agreement between the experimental hyperfine matrices and the Hartree-Fock values reported in Table V is an indication that our assumption of a hole mov-

ing in a restricted space of O $2p$ nonbonding orbitals is well justified, since the Hartree-Fock approximation is exact for a single hole in a finite orbital space. A further test of the model can be done by considering the effective single-particle Hamiltonian in the different approximations. In the restricted orbital space, this is given by

$$H_{ij}=\frac{\delta E[\rho]}{\delta \rho_{ij}}. \tag{24}$$

We consider an energy functional that is a linear combination of DFT and Hartree-Fock energies,

$$E=C+\sum_i \varepsilon_i\rho_{ii}+\frac{1}{2}\sum_{ij} U_{ij}(\rho_{ii}\rho_{jj}-x\rho_{ij}\rho_{ji})$$

$$+(1-x)\sum_i E_{\mathrm{loc}}(\rho_{ii}), \tag{25}$$

which leads to the Hamiltonian

$$H_{ij}=\left[\varepsilon_i+(1-x)\left.\frac{dE_{\mathrm{loc}}(\rho)}{d\rho}\right|_{\rho=\rho_{ii}}+\sum_k U_{ik}\rho_{kk}\right]\delta_{ij}$$

$$-xU_{ij}\rho_{ji}. \tag{26}$$

The important point to notice is, that the magnitude of the off-diagonal matrix elements is controlled by the parameter x as long as the hopping integrals can be neglected. Therefore, with a purely local xc energy functional, the Hamiltonian will be strictly diagonal, and if the hole is to be distributed over the available sites this must imply that the one-particle levels are degenerate at self-consistency. This is not necessarily the case when off-diagonal matrix elements are introduced, as will be the case for the Hartree-Fock and B3LYP energy functionals, but we would expect the energy differences of the eigenstates to follow the magnitude of the off-diagonal couplings. Therefore, our model Hamiltonian predicts that the difference in energy between the highest occupied and lowest unoccupied state should vanish when using a purely local/semilocal xc energy functional, and that the Hartree-Fock gap should be larger than that found using B3LYP. In Ref. 29 this prediction was found to be fulfilled in the PW91 supercell calculation: The lowest unoccupied band states are just the top of the uppermost valence band. In the cluster calculations, we find that the Hartree-Fock gap in the minority spin channel is 10.9 eV while the B3LYP calculation in the same atomic geometry yields a gap of 1.02 eV. This is a further indication that the assumptions behind our approximative hole energy functional, in particular, the neglect of hopping matrix elements, are sound, and also that the examination of HF and DFT eigenvalue spectra may reveal the presence of a self-interaction problem. It is interesting to notice that a difference between Hartree-Fock and DFT eigenvalues similar to the one described here was recently found by Kotomin *et al.* for a K vacancy in $KNbO_3$.[49] Also in this case, a large difference in the magnitude of structural relaxations was found between HF and DFT approaches.

IV. CONCLUSION

In conclusion, we have undertaken a theoretical investigation of the electronic and atomistic structure and hyperfine parameters of neutral substitutional Al and P impurities in α-quartz. For the P impurity, we find that DFT in a repeated-supercell geometry using the PW91 approximation yields results in good agreement with available experimental data. In the case of Al, the DFT approach is shown to fail qualitatively in describing the geometric and electronic structure of the impurity, both when using PW91 in a supercell, or when using the B3LYP functional in a cluster geometry. We have shown, that the Hartree-Fock approximation applied to the model cluster gives hyperfine parameters in excellent agreement with experiment, and argue that the failure of the DFT methods for this problem is a consequence of the incomplete self-interaction cancellation usually present in density functional theories.

ACKNOWLEDGMENTS

We thank Lars B. Hansen and the Center for Atomic-Scale Materials Physics (CAMP) for valuable guidance on the use of their plane-wave band structure program. Stimulating discussions with A. Svane are gratefully acknowledged. The use of Danish national computer resources was supported by the Danish Research Council.

[1] H. Hosono, Y. Abe, Y. L. Lee, T. Tokizaki, and A. Nakamura, Appl. Phys. Lett. **61**, 2747 (1992).
[2] K. L. Brower, Phys. Rev. B **20**, 1799 (1979).
[3] Y. Uchida, J. Isoya, and J. A. Weil, J. Phys. Chem. **83**, 3462 (1979).
[4] L. E. Halliburton, N. Koumvakalis, M. E. Markes, and J. J. Martin, J. Appl. Phys. **52**, 3565 (1981).
[5] D. L. Griscom, E. J. Friebele, K. J. Long, and J. W. Fleming, J. Appl. Phys. **54**, 3743 (1983).
[6] H. Hosono and N. Matsunami, Phys. Rev. B **48**, 13 469 (1993).
[7] D. C. Douglass, T. M. Duncan, K. L. Walker, and R. Csencsits, J. Appl. Phys. **58**, 197 (1985).
[8] K. Fukumi, A. Chayahara, M. Makihara, K. Fujii, J. Hayakawa, and M. Satou, J. Am. Ceram. Soc. **77**, 3019 (1994).
[9] M. Martini, A. Paleari, G. Spinolo, and A. Vedda, Phys. Rev. B **52**, 138 (1995).
[10] L. D. Bogomolova, Y. G. Teplyakov, A. A. Deshkovskaya, and F. Caccavale, J. Non-Cryst. Solids **202**, 185 (1996).
[11] K. Fukumi, A. Chayahara, N. Kitamura, J. Nishii, K. Kadono, M. Makihara, K. Fujii, and J. Hayakawa, J. Appl. Phys. **79**, 1060 (1996).
[12] M. Mombourquette, J. Weil, and P. Mezey, Can. J. Phys. **62**, 21 (1984).
[13] F. Sim, C. Catlow, M. Dupuis, and J. Watts, J. Chem. Phys. **95**,

4215 (1991).
[14] B. Zhang and K. Raghavachari, Phys. Rev. B **55**, 15 993 (1997).
[15] G. Pacchioni and R. Ferrario, Phys. Rev. B **58**, 6090 (1998).
[16] A. Zyubin and V. Sulimov, Glass Phys. Chem. **25**, 6090 (1999).
[17] T. Uchino, M. Takahashi, and T. Yoko, Phys. Rev. Lett. **84**, 1475 (2000).
[18] P. Hohenberg and W. Kohn, Phys. Rev. **136**, B864 (1964).
[19] W. Kohn and L. Sham, Phys. Rev. **140**, A1133 (1965).
[20] R. O. Jones and O. Gunnarsson, Rev. Mod. Phys. **61**, 689 (1989).
[21] A. Pasquarello and R. Car, Phys. Rev. Lett. **80**, 5145 (1998).
[22] M. Boero, A. Pasquarello, J. Sarnthein, and R. Car, Phys. Rev. Lett. **78**, 887 (1997).
[23] C. Carbonara, V. Fiorentini, and S. Massidda, J. Non-Cryst. Solids **221**, 89 (1997).
[24] A. Yokozawa and Y. Miyamoto, Appl. Phys. Lett. **73**, 1122 (1998).
[25] A. Oshiyama, Jpn. J. Appl. Phys., Part 2 **37**, L232 (1998).
[26] N. Capron, S. Carniato, G. Boureau, and A. Pasturel, J. Non-Cryst. Solids **245**, 146 (1999).
[27] A. Continenza and A. D. Pomponio, Phys. Rev. B **54**, 13 687 (1996).
[28] M. Magagnini, P. Giannozzi, and A. D. Corso, Phys. Rev. B **61**, 2621 (2000).
[29] J. Lægsgaard and K. Stokbro, Phys. Rev. B **61**, 12 590 (2000).
[30] G. Pacchioni, F. Frigoli, D. Ricci, and J. A. Weil, Phys. Rev. B **63**, 054102 (2001).
[31] J. Lægsgaard and K. Stokbro, Phys. Rev. Lett. **86**, 2834 (2001).
[32] G. Kresse and D. Joubert, Phys. Rev. B **59**, 1758 (1999).
[33] D. Vanderbilt, Phys. Rev. B **41**, 7892 (1990).
[34] P. Blöchl, Phys. Rev. B **50**, 17 953 (1994).
[35] C. G. V. de Walle and P. E. Blöchl, Phys. Rev. B **47**, 4244 (1993).
[36] P. Blöchl, Phys. Rev. B **62**, 6158 (2000).
[37] J. H. E. Griffiths, J. Owen, and I. M. Ward, in *Defects in Crystalline Solids; Report of the Bristol Conference* (Physical Society, London, 1954), p. 81.
[38] M. O'Brien, Proc. R. Soc. London, Ser. A **231**, 404 (1955).
[39] A. Taylor and G. Farnell, Can. J. Phys. **42**, 595 (1964).
[40] O. Schirmer, Solid State Commun. **18**, 1349 (1976).
[41] R. Nuttall and J. Weil, Can. J. Phys. **59**, 1696 (1981).
[42] A. D. Becke, J. Chem. Phys. **98**, 5648 (1993).
[43] J.P. Perdew, J. Chevary, S. Vosko, K. Jackson, M. Pederson, D. Singh, and C. Fiolhais, Phys. Rev. B **46,** 6671 (1992)
[44] G. Pacchioni and C. Mazzeo, Phys. Rev. B **62**, 5452 (2000).
[45] J. P. Perdew and A. Zunger, Phys. Rev. B **23**, 5048 (1981).
[46] A. Svane, Phys. Rev. B **53**, 4275 (1996).
[47] A. Svane and O. Gunnarsson, Phys. Rev. Lett. **65**, 1148 (1990).
[48] W. A. Harrison, *Electronic Structure and the Properties of Solids* (Dover, New York, 1989).
[49] E. A. Kotomin, R. I. Eglitis, A. V. Postnikov, G. Borstel, and N. E. Christensen, Phys. Rev. B **60**, 1 (1999).